Introduction

We report in this paper a study of the effects of atmospheric turbulence on the imaging of scenes, for an horizontal propagation of the light over a distance of 20 km, 15 meters above the sea surface. The data material is the result of a series of observations of images obtained at the focus of a 20cm telescope and analysed at visible wavelengths with a CCD camera of high sensitivity and variable integration time. Observations were made by night, on point-source targets, and in day time on a complex extended source. The results reported here mostly concerns nighttime observations.

The procedure we used to quantify the effects of the atmospheric turbulence for this horizontal propagation is mainly derived from those used in astronomy for site testing. We make use of blurring and image motion models and speckle transfer functions. Several quantities such as C_n^2, Fried's parameter r_0 or scintillation rate are obtained.

After a brief description of the site and of the observational setup in section II, the organization of the paper follows an empirical basis: Section III describes the blurring, image motion and scintillation effects of point source targets. These low frequency visible features of the effect of turbulence are interpreted in terms of the Fried's parameter. Results on the domain of isoplanatism are also given there. Information about angle of isoplanatism is retrieved in section IV from a speckle interferometry analysis of the image. Finally, the result of day time observations of a complex extended source are reported in section V and a conclusion drawn in section VI.

I. Description of the site and the observational setup

The observation were performed on the Mediterranean shore, from cap Cepet located in Saint Mandrier's peninsula, to Porquerolles's island 20km away. The optical path was 15m above the sea surface and observation were made in visible light.

For night time observations, data were mainly recorded between 18h and 06h of September 27th 1995. Regarding day time, data were recorded from the 27th of september to the 3th of November. During this last period 74% of the observing time, observations could not have been made because the transparency of air was not good enough.

The data acquisition device, shown in figure 1, consists of a telescope, a microscope objective and a CCD camera. The microscope objective is used to enhance the size of image of the telescope to fit the resolution of the CCD camera. We observed using microscope objectives of magnification x5 and x7, the use of x7objective allows to represent 0.25 arcsec. on a pixel (1.2 μrad).

The telescope used is a Celestron C8, of diameter 20cm, with a 7cm central obstruction; its theoretical resolving power is 0.6 arcsec at 0.5 μm. With the magnification used, the field of view is 44 arcsec. We used a CCD camera (IMC 85) and the image was recorded on an analog video recorder in SVHS standard.

During the night, point source target were used. The sources were positioned on two rails in a vertical plane at right angle horizontally and vertically, each one maintaining two mobiles 75Watt spots as shown in figure 2. Spots were of 5 cm diameter, that is below the limit resolving power of our system. Our device makes it possible to modify the number and position of point sources. A 500 Watt search light was also used.

II. Qualification of image quality using global observation.

The presence of atmospheric turbulence degrades the images, and it has long been known that increasing the size of a telescope beyond a certain limit does not improve the visual observation conditions. The atmosphere is considered to impose a filtering of the spatial frequencies present in an incident wave, thus limiting the effective resolving power of a ground-based telescope. The definition of image quality, which is expressed by the size of the smallest discernable detail in the image, is thus related uniquely to the state of the atmosphere irrespective of the telescope in use.

Fried [1] introduced a parameter r_0 which provides a measure of image quality and can be defined as the telescope diameter which, in the absence of atmospheric turbulence, would give the same image resolution as a telescope of infinite aperture in the presence of turbulence. The parameter r_0 may be interpreted as well as the diameter of coherent portions of the perturbed wavefront incident on the entrance pupil of the telescope. For a given telescope, the value of the Fried parameter is enough to quantify the apparent effects called blurring and image motion.

Assuming isoplanatism [2], the relationship between the intensity in the focal plane *i(x,y)* and the illumination of an object *o(x,y)* in the presence of turbulence can be written as a convolution product:

$$i(x, y, t) = o(x, y) * r(x, y, t) \qquad \textit{eq. 1}$$

where *t* represents time and *x, y* the position. The function *r(x, y, t)* is the instantaneous point spread function (PSF) of the atmosphere - instrument ensemble, for which an unresolved bright object appears at any given moment as a distribution of dark and bright spots called speckles. The angular extent of the speckles is approximately limited to $2.5\ \lambda/r_0$. The analysis of the speckle phenomenon will be described in section III.

During long exposures, the time-average of *r(x, y, t)* drawns the speckles phenomenon and the averaged transfer function acts as a low pass filter, so that only the low frequency information present in the signal is transmitted [3]. Without entering into any theoretical analysis, we give thereafter a simple heuristic explanation of these effects. We start first with the instantaneous image.

The speckles are spread in the image plane over a random surface $r_t(x,y)$ whose instantaneous shape depends on the coherence zones present on the pupil at time *t*. Their characteristic size can be associated with the blurring, and their transfer function is described by the so called “short- exposure” image as described by Fried, which is actually a long time exposure image corrected for image motion. From one instant to another, $r_t(x,y)$ changes in contrast and moves in the image plane by a factor related to the mean gradient of the phase errors present in the incident wave at the telescope pupil. This image motion decreases when the size of the telescope increases [4]. The overall, time-averaged value of $r_t(x,y)$ constitutes the long time exposure point spread function $R(x,y)$ as defined by Fried and related directly to r_0.

In Fried's theory, there is a consistency between the raw long time exposure point spread function, the image corrected for motion and the image motion itself. Given the size of the telescope, these three measures should be all related to r_0 and to a coefficient α that allows to take into account the relative importance of amplitude and phase perturbations of the wave front. Our analysis makes it

possible to check the validity of Fried's models for the particular case of horizontal propagation analysed. It is what we describe in subsection A and B. Another important global parameter for an observation is the rate of scintillation of the image, which is simply obtained in our experiment by a measure of the whole intensity observed from a source. It is described in subsection C. An important information may be obtained from the simultaneous observation of several sources, that is the isoplanatism angle. We derive this information from joint analysis of image motion and scintillation of close by sources. The results are given in section B and C.

In this paper, we make plenty use of the parameter r_0, but it may also be interesting to make use of the refractive index structure C_n^2. For spherical waves, Fried's r_0 parameter is related to C_n^2 by the relation [5]:

$$r_0 = 2.1\left[1.46k^2\int_0^L Cn^2(h)\,(\frac{L-h}{L})^{\frac{5}{3}}dh\right]^{-3/5} \qquad \textit{eq.2}$$

where h is the distance of a turbulent layer and dh an element of thickness, L is the distance between the object and the observer and k is the optical wave number.

In the case of an horizontal propagation we may considere that $C_n^2(h)$ has a constant value over the optical path [6], and the relation 2 is reduces to:

$$Cn^2 = 0.16 r_0^{-5/3}\lambda^2 L^{-1} \qquad \textit{eq. 3}$$

This relation will be used to relate r_0 and C_n^2 values in the following of this paper.

A. Determination of Fried's parameter r_0 from blurring measurements.

This section presents a measurement made among a large set of data were we measured Fried parameter's values between 1.5cm up to 3.6cm. As an example we choose to present especially the one we found to be the more representative for marine turbulence conditions.

We give the values of r_0 from blurred observations of PSF's with and without correction of image motion. Fried gives his results at the level of the Optical Transfer Function (OTF), Fourier transform of the PSF.

For long exposure time and monochromatic observations, the expression of the OTF is:

$$\tau_{LE}(f) = \tau_0(f)\,exp\left[-3.44\left|\frac{\lambda f}{r_0}\right|^{5/3}\right] \qquad \textit{eq. 4}$$

where $\tau_0(f)$ is the diffraction-limited OTF of the telescope, that can be written as the autocorrelation function of the telescope pupil. The PSF can be obtained as the inverse two-dimensional Fourier transform of this expression. We shall denote this PSF as $r_{LE}(x, y)$.

The second approach consists of using Fried's model for images corrected for image motion. Fried assumes that the image motion follows a Gaussian distribution in the focal plane. He deduces from this assumption that eq. 4 is the result of a filtering by a Gaussian law in the Fourier plane. The corresponding short exposure time MTF, in the sense of Fried, can be written as [2]:

$$\tau_{SE}(f) = \tau_0(f)\, exp\left[\left(-3.44\left|\frac{\lambda f}{r_0}\right|^{5/3}\right)(1-\alpha|\lambda f/D|^{1/3})\right] \qquad eq.\ 5$$

where D is the diameter of the imaging optics and α is a parameter that may vary from 1, when only phase effects are considered (near field), to 0.5 when amplitude and phase effects are both important (far field). According to Fried [1], the parameter α is a function that varies with *f*; it may be taken as a constant for given experimental conditions. The difference between the two extreme cases can be made by a comparison between the diameter of the telescope *D* and the quantity $(L\lambda)^{1/2}$, where L is the length of the propagation path through the turbulent medium. The parameter α take the value 1 for $D>>(L\lambda)^{1/2}$ corresponding to the near field case and the value 0.5 for $D<<(L\lambda)^{1/2}$ corresponding to the far field case. Our experimental conditions are typically in the intermediate case, $(L\lambda)^{1/2}$ being of the order of 10cm for a telescope diameter D=20cm, and we may expect to find a value of α lying in the range 0.5 to 1.

As for the above relation 4, the corresponding short time exposure PSF $r_{SE}(x, y)$ can be obtained as the inverse two-dimensional Fourier transform of equation 5. In fact, there is a problem for the raw application of this formula and its inversion for α=1. Indeed, in relation 5, the term $(1-\alpha(\lambda f/D)^{1/3})$ of the exponential reduces to zero when *f* reaches the cut-off frequency D/λ and, consequently, makes the exponential term equal to 1 while it should tend toward zero there. In fact Fried's correction factor is valid only for low frequency values. We used eq. 5 for a limited range of *f* values, limiting the correcting factor $(1-\alpha(\lambda f/D)^{1/3})$ to a minimum value of 0.1.

If no a priori assumptions are made on the relative importance of amplitude and phase effects, the fit between theory and experiment in the short exposure case requires the determination of the two parameters r_0 and α. Our approach was to trust the r_0 value obtained in the long exposure experiment and use it in the short exposure case to deduce the α value that best fit the observations.

The comparison between data and models was made using a set of 800 images recorded around midnight in clear air and windy conditions. The LTE image of the three sources represented in the configuration of figure 2 is represented in figure 3. A slice of the average of the raw images and a slice of the average of the recentered images are represented in figure 4. These curves are then compared with corresponding theoretical models in the next two figures.

In figure 5, curve A of figure 3 i. e., the LTE experimental result is compared with a set of LTE PSFs obtained by a 2D Fourier Transform of relation 4 for various r_0 values. The best fit, in

the least square sense, is obtained for r_0=2cm (C_n^2=1.94 10^{-15} $m^{-2/3}$).

In figure 6, curve B of figure 3, i. e. the STE experimental result is compared with a set of STE PSFs obtained by a 2D Fourier Transform of relation 5, for a fixed r_0 value of 2cm and variable α values from 0.5 to 1. The best fit in the least square sense is obtained for α=0.6.

B.1. Determination of Fried's parameter r_0 from image motion measurements.

The image motion can be directly measured from the set of images as the wandering of the photocenter of each short exposure image. Histograms of the horizontal and vertical motions are given in figure 7. The image motion presents an overall amplitude of 40μrad, equivalent in the object plane to about 80cm. There is a spread of the image motion slightly larger in the horizontal direction than in the vertical one, the standard deviations σ being respectively of 6.8μrad and 6.6 μrad for the two directions.

Assuming isotropy, the standard derivations σ of this Gaussian distribution is related to the observational conditions by:

$$\sigma^2 \approx 0.18\alpha \cdot \left(\frac{\lambda}{D}\right)^{\frac{1}{3}} \left(\frac{\lambda}{r_0}\right)^{\frac{5}{3}} \qquad \textit{eq. 6}$$

This result is drawn from relations 7.54 and 7.47 of Roddier [7], assuming identical variance of the angle of arrivals in horizontal and vertical directions. The coefficient α is used here to drop the near-field approximation used by Roddier.

A quite good consistency is found between measurements and the theoretical curve for r_0=2cm and α=0.6 leading to σ=6.7μrad. The comparisons are shown in figure 8.

B.2 Check of the isoplanatic angle for image motion

Our target made of three points sources separated from 1.7m made it very easy to check the correlation of image motions between the sources. As recently discussed by Beran and Ozvogt[6], a simple condition of isoplanatism may be to impose that the propagation of the light coming from two points sources remains with an horizontal distance much less than r_0. This condition is far to be verified in our experiment, and we must expect the image motions to be uncorrelated.

The procedure we used to check this point was to represent the probability density function (PDF) of the difference of observed positions between two close-by sources. There are two opposite cases. If the sources are viewed within an angle lower than the isoplanatic angle, their image motion should be identical. The PDF of differences of positions should be represented by a simple point at the true difference of position of the sources.

If the sources have a separation angle much greater than the isoplanatic angle their motion

become uncorrelated. In that case, we expect that the PDF of their difference of position becomes equal to the convolution product of their individual motion law of probability. In such a case, assuming for the image motion a Gaussian distribution of standard deviation σ (equation 6), we expect to obtain a Gaussian PDF of standard deviation $\sigma_{**}=\sigma\sqrt{2}$ for the differences of positions.

The comparison between experimental data and the expected theoretical model is made in figure 9. We have represented the differences of positions between the observed positions of sources S_1, S_2 and S_3 of figure 2 and 3. The observed 2D histograms are compared with the Gaussian PDF corresponding to the uncorrelated case by drawing a circle of diameter $D = 2\sqrt{2\sigma^2_{**}\, log(2)}$ of 22.2µrad that should contain 50% of the differences of positions. The obtained results (54.2% for D_1-D_2, 54.6% for D_2-D_3, and 47.5% for D_1-D_3) are roughly consistent with the assumption of uncorrelated image motions and we must conclude that the condition of isoplanatism is not satisfied for the 1.7m separation. However, the results obtained for D_1-D_2 and D_2-D_3, corresponding to the 1.7m separation might be consistent with a very small residual rate of coherence that is no more visible for the histogram corresponding to the difference of displacement D_1-D_3 corresponding to a separation of 2.38 m. Moreover, these histograms slightly depart from the expected theoretical isotropic distribution. There is a spread in the direction of the sources. This measurement of differences of positions is an indirect test of the reliability of the measurements made in section B.1.

As a result, we found that the isoplanatic angle was much less than the separation angle of the sources. We notice as well, that the fluctuation in the longitudinal direction (parallel to the base) are larger than in the transverse direction (orthogonal to the base). One should notice that such a differential method does not take into account correlated move of images caused by large scale phenomena. For instance it cannot measure the effect of a convective cell of dimensions larger or equal to the separation of the source moving in the source plane or also of a convective cell of the dimension of our pupil moving in the pupil plane.

C. Scintillation-Isoplanatic Angle

We made scintillation measurements for a single source, and analysed the correlation that exists between close by sources. The scintillation of a source produced by the atmospheric turbulence is measured as the variation of the intensity received by a point like detector located on the impinging wavefront [8].

The measurement we performed is made in the focal plane of the telescope. It consists of measuring the whole intensity received from a point source by integrating the intensity of the whole PSF. This corresponds in practice to the integration of a domain of 0.1mrad centered on the source. As a consequence, we can only measure the resulting scintillation of the light integrated over the entrance aperture of the telescope. Figure 10 shows the evolution of the received intensity as a function of time, for a total duration of 16 seconds, sampled at the standard video sample of Δt_s= 20ms. Very strong fluctuations were observed that we compare with the theoretical expectation below.

To quantify the strength of turbulence, the theory of optical scintillation uses the scintillation index defined as the ratio of the variance of the intensity to the square of its mean:

$$\sigma_I^2 = \frac{\langle S^2 \rangle - \langle S \rangle^2}{\langle S \rangle^2} \qquad \textit{eq. 7}$$

We measured σ_I^2 values of the order of 0.75. This value is very high if we consider the integration effect of large aperture. According to Bass et al. [9], it is possible to recover the magnitude of the pupil averaging effect through a coefficient *A* defined as:

$$A = \frac{\sigma^2(D)}{\sigma^2(0)} \qquad \textit{eq. 8}$$

where $\sigma_I^2(D)$ is the variance of the relative irradiance fluctuation measured with a pupil size of diameter *D* and $\sigma_I^2(0)$ the one measured with a point-like detector.

To obtain the value of *A*, we used the curve given by Bass et al. (figure 3 of [9]). Depending of the value we assume for the inner scale l_0, we can deduce that *A* range between 0.2 and 0.3. In that case, the observed $\sigma_I^2(D)$ value of 0.75 corresponds to possible $\sigma_I^2(0)$values ranging between 2.5 and 3.75. If we use the variance of the log amplitude σ_χ^2, with $\sigma_I^2 = 4\sigma_\chi^2$ [7] , we derive that this later quantity varies between 0.93 and 0.625. This possible variation is well inside the interval of values($\pi^2/24$, 1) defined by Churnside [10] for the saturation domain. According to figure 4 of Hill and Clifford [11], it is possible to locate our measured point either in the bump either in the beginning of the saturation zone. We can exclude the weak turbulence regime where a raw application of the Rytov model for the variance σ_χ^2 for a spherical wave is:

$$\sigma_\chi^2 = 0.124 k^{7/6} L^{11/6} C_n^2 \qquad \textit{eq. 9}$$

would have given a value of 2.86 for σ_χ^2 using the C_n^2 measured in above section II.A.

The variation of the integrated intensity coming from two sources is shown in figure 10 as a function of time. Strong uncorrelated fluctuations are visible from a sample to another, leading us to conclude that the scintillation correlation time is much smaller than 20 ms of time, as expected [12].

Generally, one recognize periods of strong fluctuations of the two sources (for example in the zone 0 to 2 second, and just after 8second) and periods of relatively quieter conditions clearly showing the non stationarity of the phenomenon.

As we did for the image motion in the former section, we also study the correlation of scintillation between two close-by sources. This comparison is performed using the couples of sources 1.70m *(85*μ*rad)* spaced whose scintillation is shown in fig. 10. One can note the uncorrelated fluc-

tuation of the two sources directly in this representation. This appears clearly in the correlation diagram shown in fig. 11, together with the regression lines. As a result, we may conclude that the scintillation isoplanatism domain is smaller than 1.7m for this 20km horizontal propagation.

III. Seeing parameters derived from speckle analysis.

The results obtained in the former section can be verified and completed making use of a speckle interferometric analysis of the images. The speckle technique was proposed by Labeyrie [12] for the recovery of high angular resolution in ground based optical astronomy. Its main feature consists of computing the spatial power spectrum $<|\tau(f)|^2>$ of the instantaneous images observed at the focus of the telescope. This quantity, unlike the OTF's $\tau_{LE}(f)$ and $\tau_{SE}(f)$ described in the previous section, is known to contain information up to the cut off frequency of the telescope. A very simple analytical expression for $<|\tau(f)|^2>$ can be derived if the complex amplitude of the wave at the telescope aperture is assumed to follow a circular Gaussian statistics [13]:

$$\langle|\tau(f)|^2\rangle = \tau_0^2(\lambda f)\, exp\left[\left(-6.88\left|\frac{\lambda f}{r_0}\right|^{5/3}\right)\right] + \tau_0(\lambda f)\cdot 1/N \qquad \textit{eq. 10}$$

where N is the average number of speckles per PSF, that can be written as $N= (D/r_0)^2/0.44$. The term $1/N\ \tau_0(f)$ extend up to the cutoff frequency D/λf.

In fact, it is well know to astronomical observer that this relation is too simple to truly account for the effects of the atmosphere. Several quantities should be considered; in particular, the speckle technique assumes instantaneous images, although images are necessarily recorded over a finite exposure time. A problem is to know how short must be the exposure time to observe this phenomenon. The characteristic time τ_0 for a modification of the shape of a speckle is called the “boiling time” [14], by reference to the visual appearance of the speckle image. Speckles boiling times are generally found of the order of 5 to 20ms in astronomy. The image detection system we have is not fast enough to sample in time the speckle evolution, since our data recording system is based on the standard television rate of 50 images/sec. We can however modify the integration time of each image, and therefore check the effect on the resulting image, or more precisely, on the power spectrum. This was done by performing records with several exposure time.

When the exposure time becomes larger than τ_0 , the quantity $<|\tau(f)|^2>$ decreases and tends towards $\tau^2_{LE}(f)$ for a very long exposure time. An example of the results obtained with exposure times of 4, 8 and 10ms is shown in figure 12. The data obtained with the 10ms exposure time start to present a lack of energy.

These curves correspond to successive records for which the parameter τ_0 may of course have varied. We may however conclude that the regular integration time of 20ms of a classical television image is not short enough to freeze the atmospheric turbulence while an integration time of 4ms seems to be a safe value. For the experiment reported here, curves obtained for 4ms and 8ms

are close enough to assume a τ_0 value of the order of 8ms.

Beside these considerations, the curves reported in figure 12 are the result of a sophisticated treatment in order to get rid of the photodetection bias noise that would appear as a white frequency contribution. The corresponding procedure is described in the Annexe.

Expression 8 might be used to fit the observations and derive from it the parameter r_0. In fact, the raw comparison is unsatisfactory, and several effects may be taken into account. One is the effect of the wavelength.

Our observations were made in white light, with a S(λ) sensitivity detector ranging from 0.4 μm to 1μm. With the very crude assumption that the speckles are correlated over this range of wavelength for this small telescope, we can write an average transfer function in white light of the form:

$$\langle |\tau(f)|^2 \rangle_{WL} \approx \int \langle |R_{LE}(\lambda f)|^2 \rangle \cdot S(\lambda)\, d\lambda \qquad \textit{eq. 11}$$

This curve was used to fit the observations. The consistency is not very good. Using mainly the low part of the curve (figure 13) we obtained a value of r_0 of 2cm which is consistent with blurring measurements.

In figure 13 we note a poor agreement for the intermediate range of spatial frequencies, this difference could be due to several effects, such as a defocus or a default of the model which does not consider chromatic decorrelation. Part may be also due to our data acquisition device, which goes through an analog video recorder.

We have also checked the isoplanatism domain for the speckle experiment by computing the cross spectrum between instantaneous images of the form $< \tau_1(f)\, \tau^*_2(f) >$, where $\tau_1(f)$ and $\tau_2(f)$ are the Fourier Transform of the speckle patterns simultaneously produced by the sources S_1 and S_2 at the telescope focus. The symbol "*" stands for complex conjugate. This curve is reproduced in figure 14 where it is compared with a cross spectrum obtained between images separated in time by 8seconds, and that we expect to be fully uncorrelated. The image power spectrum is also represented.

The results support the conclusion derived in section II. In a first approximation, PSFs corresponding to point sources separated by 1.7m are uncorrelated, as it can be seen from the comparison between $<\tau_1(f)\, \tau^*_2(f)>$ and $<|\tau(f)|^2>$. However, we cannot exclude some residual correlation, since the cross spectrum corresponding to simultaneous images presents slightly more power in the high frequencies than the one computed for long time lagged images. It may be also interesting to note that the default of isoplanatism does not influence the OTF in the low frequency range.

IV. Daytime Observations.

During daytime observations, we used the rectangular object of dimension 4x3 m represented in figure 15. The images were recorded in the afternoon, from 1 to 6 pm during nine days, from September 26th to November 13th when transparency of air was satisfactory. Indeed, the daytime

observation were strongly affected by the turbidity phenomenon, so that observation was impossible during about 74% of the time.

When the atmosphere was clear enough, we carried out a measurements of r_0 based on the spread of the edges of our object, following the method indicated thereafter.

We average first the image of an edge of the object, next, we consider a slice view orthogonal to the edge direction (figure 16 (a)), we compute the derivative of this slice. Thus obtaining the integral of the raw PSF in one dimension.

In a formal way we have:

An edge may be represented by an Heavyside function H(x) and the LE PSF by the function S(x,y). The slice view of an integrated image is written as:

$$U(x) = \{ H((x) * S(x,y)) \} \delta(y) + b(x) \qquad \textit{eq. 14}$$

where δ(y) is the direction of the slice, b(x) represent an additive noise term. The derivation of the slice is:

$$U'(x) = \{ \delta(x) * S(x,y) \} \delta(y) + b'(x) \qquad \textit{eq. 15}$$

equivalent to:

$$U'(x) = \int S(x,y)\, dy + b'(x) \qquad \textit{eq. 16}$$

Thus we obtain an experimental value of the integral of the raw PSF in one dimension.

We can now use the previously defined Fried's long exposure model to obtain by inverse Fourier Transform a theoretical expression equivalent to *U'(x)*.We determine r_0 as the value giving the best fit in the least square sense between theoretical and experimental values of *U'(x)*.

Using such a method we measured Fried parameter value ranging from 3.6cm to less than 0.5cm. Typical conditions are found to be of the order of 1.5cm.

In good condition of air transparency, we observed distorsions of our rectangular object in a way similar to what is currently observed by solar astronomers on the solar limb at sunset. There is a general perturbation of the image, producing wavelike distorsions along horizontal edges and some kind of boiling like distortion for the verticals edges. These distorsions seems to be drawn by the wind.

V. Conclusion

We have reported in this paper the result of a series of observations of the effects of the atmospheric turbulence on the imaging of scenes, for an horizontal propagation of the light over a distance of 20km, 15 meters above the surface of the sea. The image formed at the focus of a 20cm telescope was analyzed at visible wavelength with a CCD camera. Observations were made during the night and on daytime.

During the night, a target made of three point sources was used. The characterisation of image quality was first made using global observations of blurring, image motion and scintillation of these point sources. The parameter of Fried r_0 was deduced from the raw long time exposure point source image and the one corrected for image motion. A typical value of 2cm was found for r_0 using Fried's theory for blurring. The image motion was directly measured as the wandering of the photocenter of each short exposure image. This measurement shows standard deviations of about 6.7 μrad, slightly larger in the horizontal direction than in vertical one. The value r_0 derived from image motion alone is in agreement with the former one for a Fried's coefficient α of 0.6 corresponding to intermediate conditions between far field and near field. These observations were completed by scintillation measurements. These measurements were obtained by simply integrating the image of a point source at the focus of the 20cm diameter telescope. We found an integrated scintillation index of the order of 0.75, which corresponds to a saturation mode for the intensity of the wave at the telescope aperture.

The use of several point sources made it possible to check the isoplanatism angle. This was made from image motion and scintillation measurements of close by sources. Although theory predicts a very small isoplanatic domain, of the order of r_0 in the target plane, a very weak residual correlation was found between sources separated by 1.7m

This analysis was completed using speckle measurements. An estimate of the boiling time was obtained from the analysis of the power spectrum of images recorded with different integration times. A typical value of 4ms seems to be sufficient to freeze the speckle image. The r_0 values obtained from speckle measurements confirmed the previous ones for which global observation were used. Speckle analysis also confirmed the measurements concerning the residual correlation for the isoplanatic domain at 1.7m.

The daytime observations reported here are the results of a preliminary approach; however they already show clearly the very poor seeing conditions and the presence of distorsions similar to those currently observed for the solar limb at sunset.

ACKNOWLEDGMENT

We would like to thanks Alexandre Robini for the help given in the construction of the instrumental device. Thanks are also due to Jean Vernin, Julien Borgnino and François Martin and to Gilbert Ricort, Paul Massiani, Marco Barilli and Alessandro Barducci for assistance during observations.

Annexe I

We briefly describe in this annex the technique we used to get rid of the noise bias in the determination of the power spectrum $< |\tau(u)|^2 >$and the autocorrelation function[15].

Assuming independence between noise and signal, the power spectrum can be written:

$$\langle |R(u)|^2 \rangle = \langle |S(u) + N(u)|^2 \rangle = \langle |S(u)|^2 \rangle + \langle |N(u)|^2 \rangle \qquad \textit{eq. A. 1}$$

The technique we used to suppress the noise in power spectrum consisted in splitting the data r(x) given by a single channel in two set corresponding to odd $r_o(x)$ and even $r_e(x)$ line of the spatial sample. If we assume that the sampling of $r_e(x)$ include the zero point, then we can considere $r_o(x)$ as the sample which would have been obtained for the signal shifted by an angular displacement “a” which is to the sampling interval. We can write $r_o(x)$ and $r_e(x)$ in the form:

$$r_e(x) = s(x) + n_e(x) \qquad \textit{eq. A. 6}$$

$$r_o(x) = s(x+a) + n_o(x)$$

By noting that the Fourier transform of the s(x+a) is given by S(u).exp-2iπau, the interlaced cross-power spectrum becomes:

$$\langle R_e(u)\, R_o^*(u) \rangle = \langle |S(u)^2| \rangle \cdot e^{2i\pi au} \qquad \textit{eq. A. 7}$$

After correction for the deterministic phase term 2iπau, the cross power spectrum give an unbiased estimate for $<|S(u)|^2>$.

REFERENCES

[1] Fried D L 1966 *J. Opt. Soc. Am.* **56** 1372-1379
[2] Goodman J W 1985 *Statistical Optics*
[3] Korff D, Dryder G, and Miller M G 1972 *Opt. Commun*. **5** 187
[4] Ziad A, Borgnino J, Martin F,Agabi K 1994 *A&A* Vol. 282 1021-1033
[5] Tofsted D H 1991 *SPIE* 1487 372
[6] Beran M J and Oz-Vogt J *Progress in Optics* Vol. XXXIII 319-388
[7] Roddier F 1981 *Progress in Optics* Vol. XIX 281-376
[8] Vernin J 1979 *thesis of University of Nice*
[9] E. Bass, B. D. Lackovic and L. C. Andrews 1995 *Optical Engineering* **34** 1
[10] Churnside J H 1990 *N.O.A.A.*
[11] Hill R J and Clifford S F 1981 *J. Opt. Soc. Am.* **71**

[12] Labeyrie A 1970 *Astron. Astrophys.* **9** 85-87
[13] J. C. Dainty 1975 *Topics in applied Physics* **9** 255-280
[14] Roddier F, Gilli J M, Lund G 1982 *J. Optics* 13-5
[15] Aime C. 1988 *Tenth Sacramento Peak Summer Workshop* 177-185

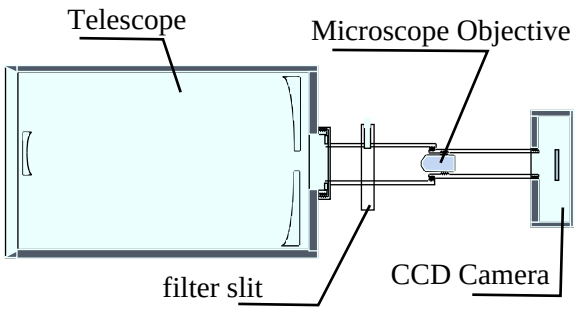

Fig 1

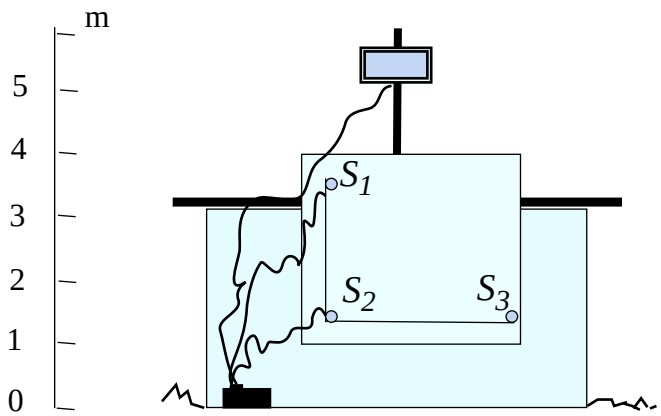

Fig 2

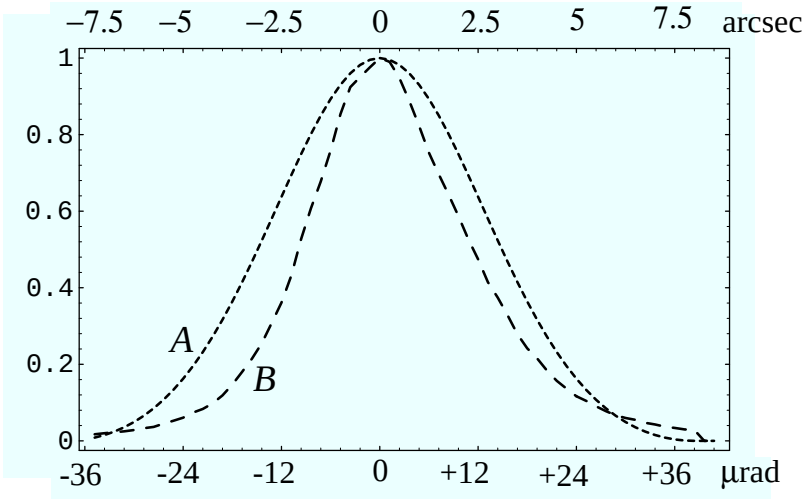

Fig 4

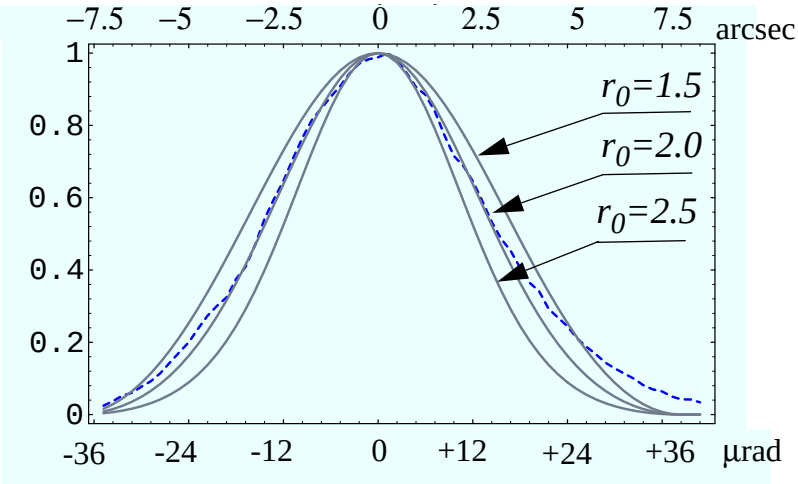
−7.5
−5
−2.5
0
2.5
5
7.5
arcsec
1
0.8
0.6
0.4
0.2
0
r_0=1.5
r_0=2.0
r_0=2.5
-36
-24
-12
0
+12
+24
+36
μrad

Fig 5:

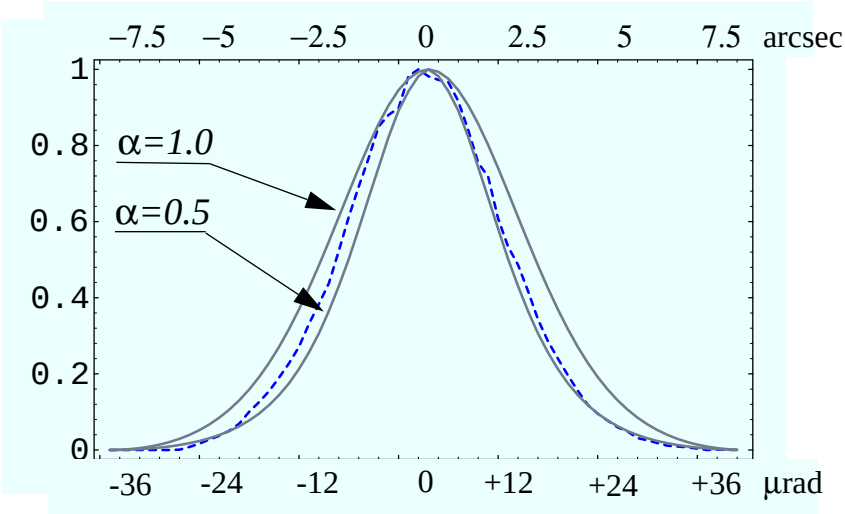
–7.5
–5
–2.5
0
2.5
5
7.5
arcsec
1
0.8
0.6
0.4
0.2
0
α=1.0
α=0.5
-36
-24
-12
0
+12
+24
+36
µrad

Fig 6

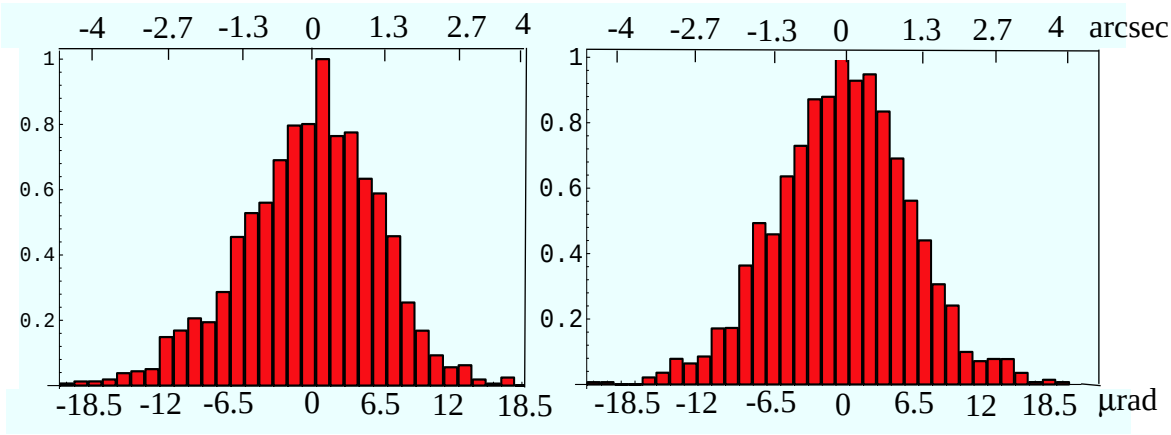

Fig 7

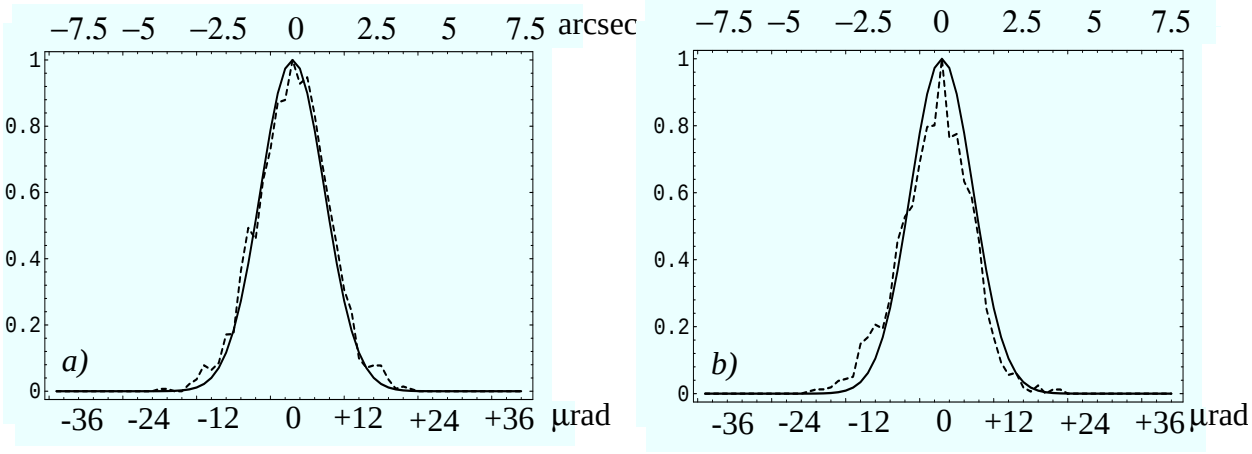
–7.5 –5 –2.5 0 2.5 5 7.5 arcsec
1
0.8
0.6
0.4
0.2
0
a)
-36 -24 -12 0 +12 +24 +36 µrad
–7.5 –5 –2.5 0 2.5 5 7.5
1
0.8
0.6
0.4
0.2
0
b)
-36 -24 -12 0 +12 +24 +36 µrad

Fig 8

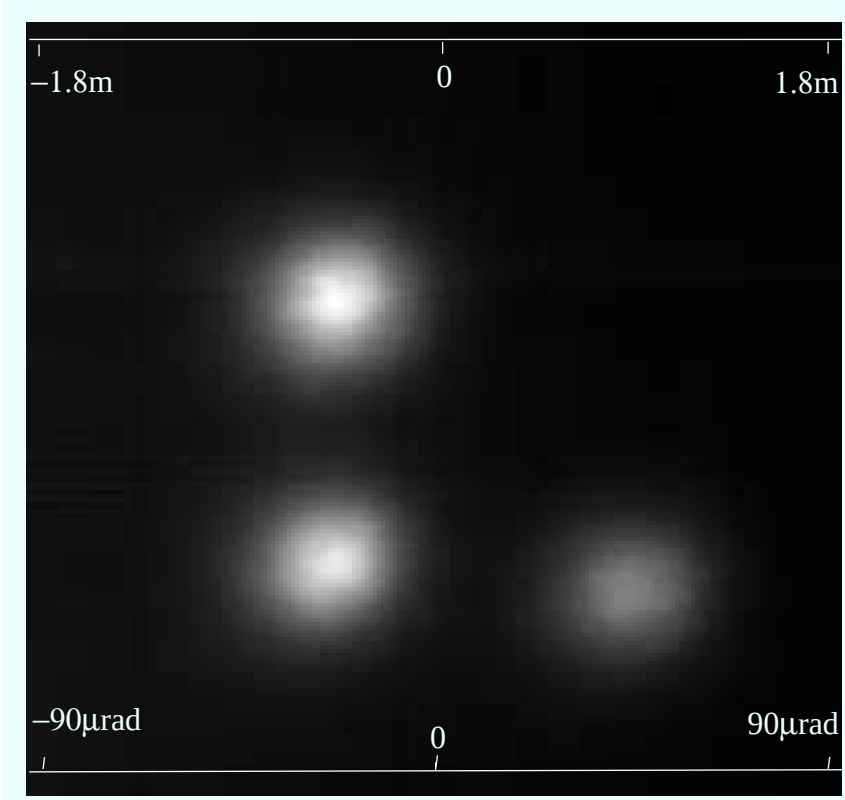

Fig 3

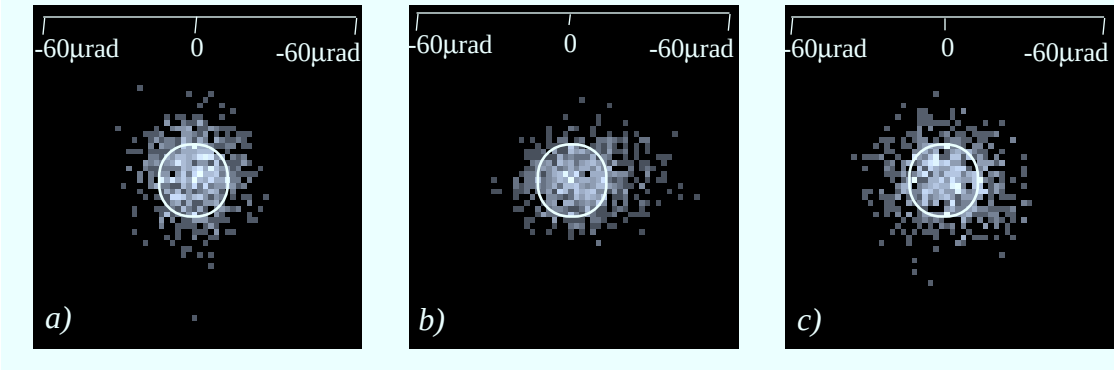

Fig 9:

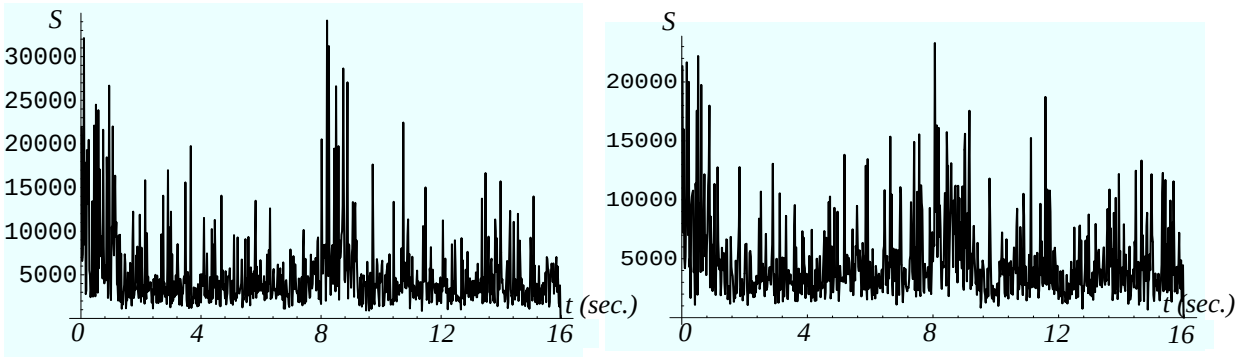
S
30000
25000
20000
15000
10000
5000
0
4
8
12
16
t (sec.)
S
20000
15000
10000
5000
0
4
8
12
16
t (sec.)

Fig 10:

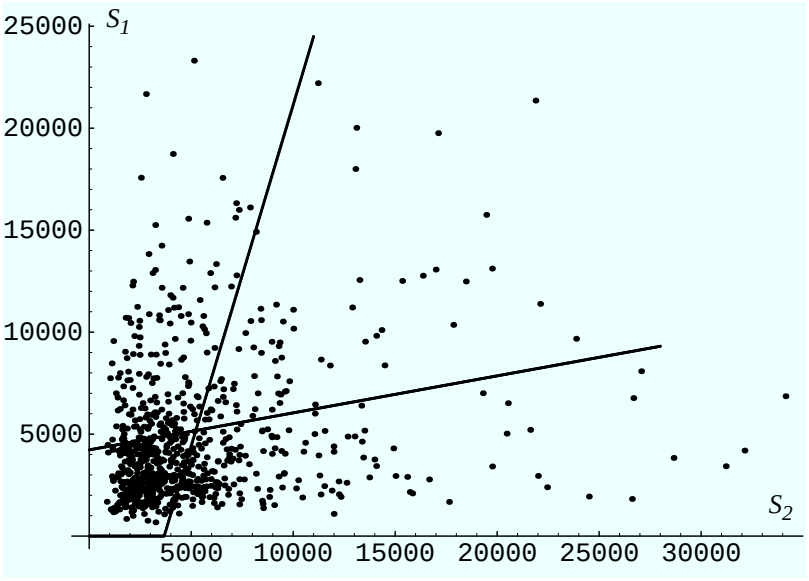
S_1
25000
20000
15000
10000
5000
S_2
5000
10000
15000
20000
25000
30000

Fig 11:

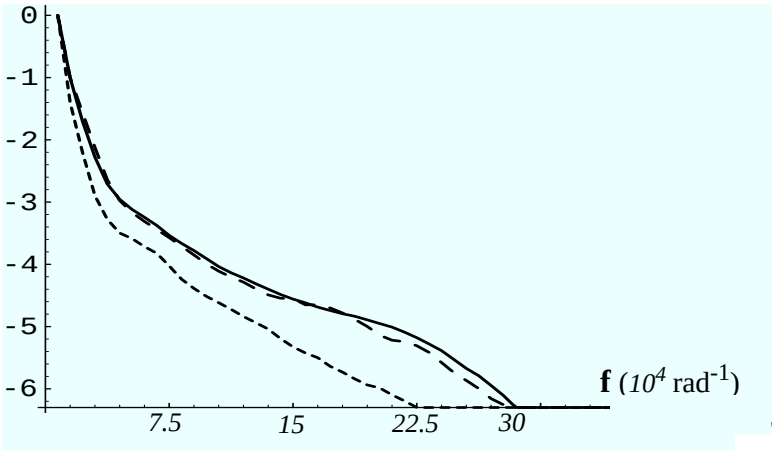

Fig 12:

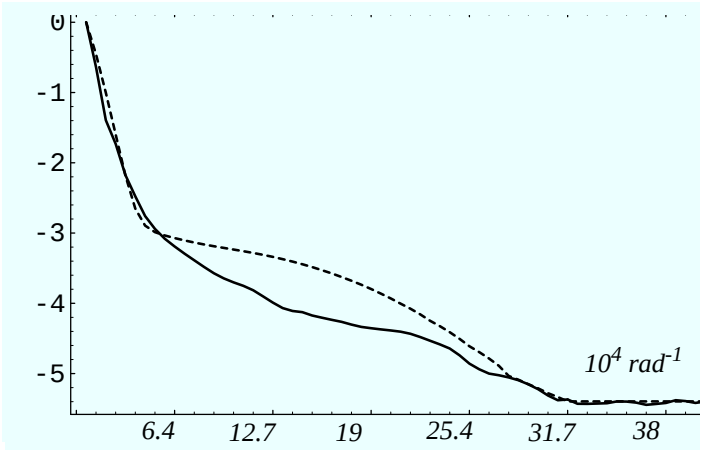

Fig 13:

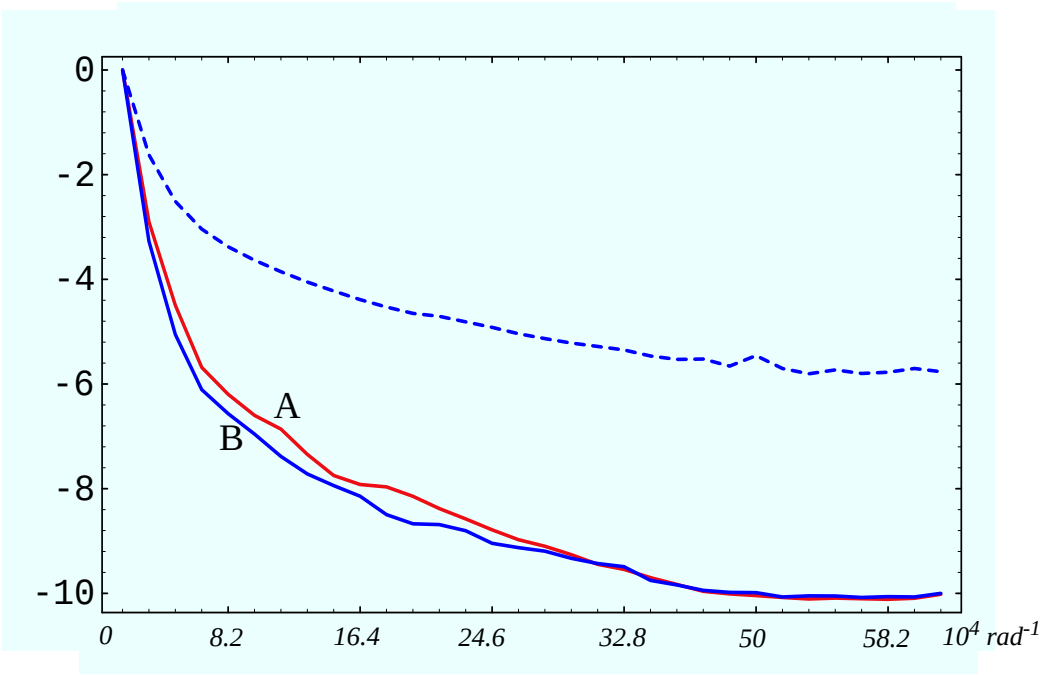

Fig 14

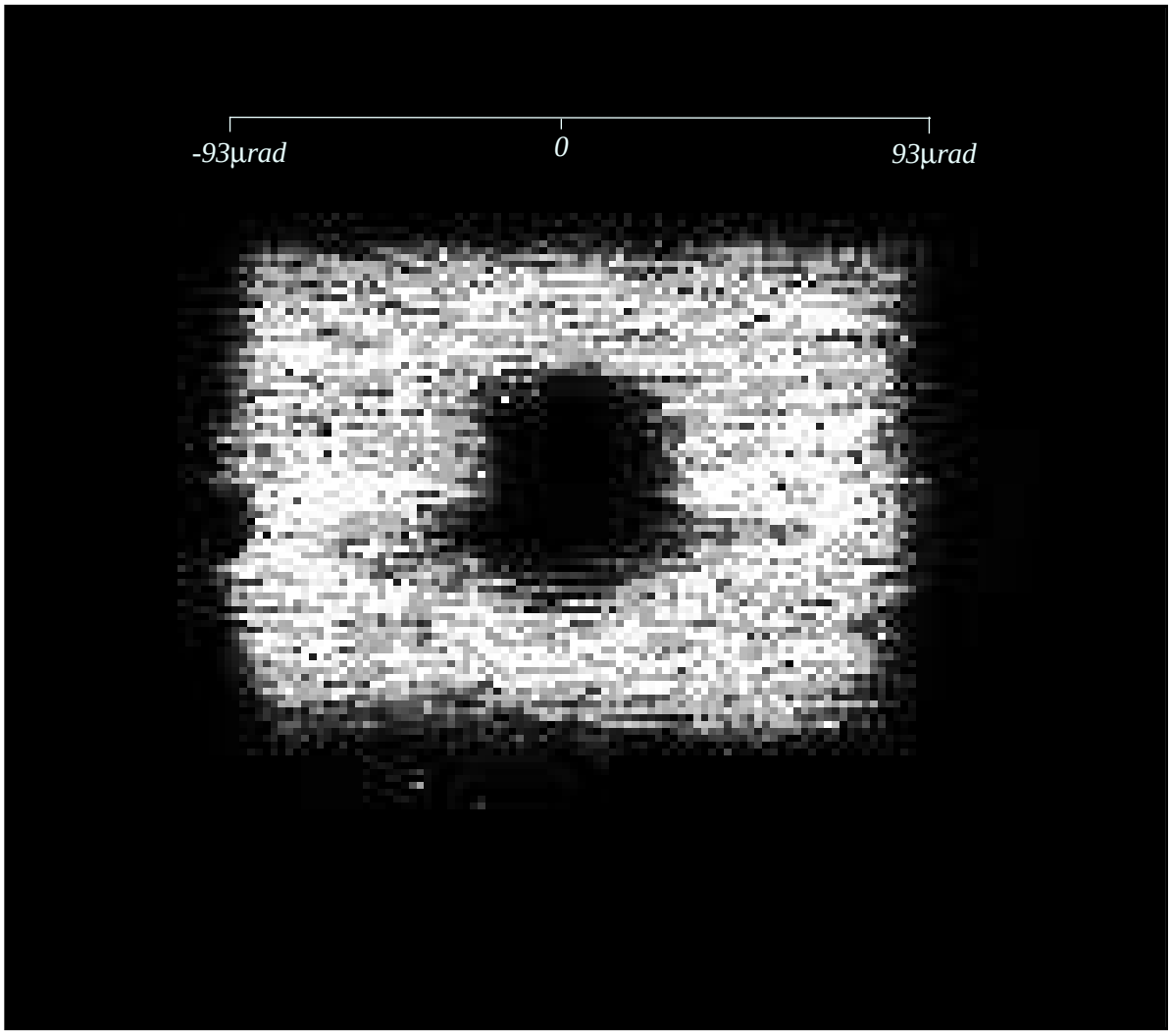

Fig 15

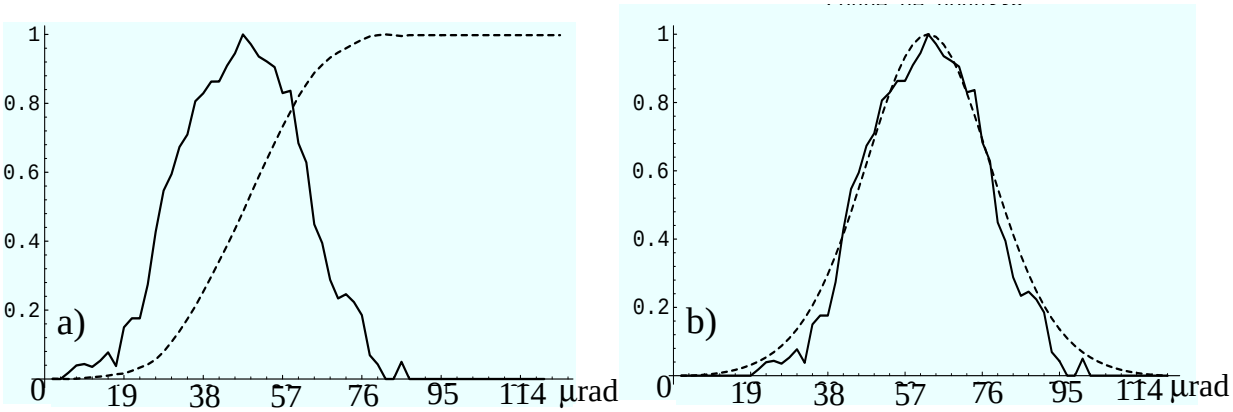
1
0.8
0.6
0.4
0.2
a)
0
19
38
57
76
95
114 µrad
1
0.8
0.6
0.4
0.2
b)
0
19
38
57
76
95
114 µrad

fig 16

List of Captions for illustrations

Fig 1: Data acquisition device: at the focus of a Celestron telescope, a microscope objective is used to form an enlarged image on a I2S CCD *camera. A filter may be used to restrict the spectral bandwidth.*

Fig 2: Configuration of the objects for night-time observation: three spots (S_1, S_2, S_3) can be moved horizontally and vertically on a large panel below a fixed search light.

Fig 3: Average of 800 instantaneous images of the three sources, distants one another from 170cm, corresponding to an angle of 85µrad for the target set at 20km of the observer.

Fig 4: Comparison between slices of a raw long exposure image (short dotted line A) and the same observation corrected for image motion, called short exposure image in Fried's terminology (large dotted line B).

Fig 5: Comparison between a slice of a long exposure image (dotted line) with Fried's model for different values of r_0.
The best fit (dotted line) is obtained for r_0= 2cm (Cn^2= 1.94 10^{-15} $m^{-2/3}$).

Fig 6: Comparison between a slice of a short exposure image with Fried's model for r_0= 2cm (Cn^2= 1.94 $10^{-15}m^{-2/3}$) and different values of the α parameter
The optimal value of α is about 0.6.

Fig 7:Histograms of the position of the photocenter of an unresolved source: left, Vertical image motion; Right horizontal image motion.
The unit interval on the abscisse axis represents a 1.2µrad shift.
The zero is set at the overall average position.

Fig 8: Comparison between the image motion histogram (doted line) and the Gaussian law corresponding to r_0= 2cm, or Cn^2= 1.94 10^{-15} $m^{-2/3}$ (full line).
Left: vertical image motion; right: horizontal image motion.

Fig 9: Differences of observed positions of the 85µrad separated sources.
From left to right: along vertical (S_1-S_2), horizontal (S_3-S_2) and diagonal (S_1-S_3) baseline.
The circle superimposed to the figure represent the limit of 2D Gaussian PDF such that the two dimensional integral is 0.5. The measured values are 54.6% for (D_1-D_2), 54.2% for (D_3-D_2) and 47.5% for (D_3-D_1).

Fig 10: Scintillation: comparison of integrated irradiance of two sources 170cm (85µrad) spaced.
The sample rate, Δt_s, is the video standard 20ms sample.
N=800 measurements are represented corresponding to 16 seconds of time..

Fig 11: correlation diagram of the integrated irradiance of close by sources with the two linear regression lines (data of figure 10).

Fig 12: *Comparison between power spectra obtained with different exposure times (semi logarithmic scale).*
Short doted line: exposure time of 10ms; Long doted line: exposure time 8ms.
Full line: exposure time:4ms. Thus for an exposure time of 4ms the images could be considered frozen

Fig 13: Comparison between speckle power spectra: full line: observation, dashed line: normal model as given by eq. 8 and 9 with r_0*= 2cm.*

Fig 14: Comparison betxeen power spectrum of a source (dotted line), cross spectrum of instantaneous images (A) and cross spectrum of obtained with images separated in time (B). One note a residual correlation for instantaneous images.

Fig 15: Day-time image of an extended object represented on a panel of 4 metres long and 3 metres high. The effects described in the body of the paper are visible only when looking to a movie.

Fig 16: Day time observations.
a) The dotted curve represents a sliced view of the LTE image of an edge blurred by the 2D PSF. The full line curve is its derivative, i. e. the integral of the 2D PSF in a direction orthogonal to the edge.
b) Comparison of the previous curve, with the theoretical result deduced from the LTE Fried's model. The best fit is obtained here for r_0*= 1.5cm.*